Role of Matter Interactions in Superradiant Phenomena

João Pedro Mendonça,[1,*] Krzysztof Jachymski,[1,†] and Yao Wang[2,‡]
[1]*Faculty of Physics, University of Warsaw, Pasteura 5, 02-093 Warsaw, Poland*
[2]*Department of Chemistry, Emory University, Atlanta, Georgia 30322, USA*

(Received 6 March 2025; revised 25 June 2025; accepted 5 September 2025; published 23 September 2025)

The superradiant phenomenon, usually described by the Dicke model, is a hallmark of strong light-matter interaction. We explore how matter-matter interactions influence this phenomenon by performing ground-state simulations of Dicke-like models with both isotropic and anisotropic interactions. We find that Ising-type interactions produce two qualitatively distinct phase boundaries, one of which gives rise to an antiferromagnetic-normal phase connected to the superradiant regime via a first-order phase transition. Under anisotropic couplings, we uncover a strongly correlated phase where in-plane spin order coexists with superradiance, exhibiting sublinear scaling of the photon occupation per site and power-law decay of spin correlations. Furthermore, superradiance is strengthened by tuning either isotropic or anisotropic interactions, highlighting the role of intrinsic many-body correlations in shaping light-matter quantum phases.

DOI: 10.1103/z8gv-7yyk

Coupling a macroscopic ensemble of quantum emitters to a common electromagnetic mode gives rise to collective phenomena such as photon-mediated entanglement and superradiant photon condensation. These effects underlie emerging technologies in quantum computing, simulation, communication, and sensing [1–7]. More recently, these systems have inspired new paradigms such as quantum batteries, which aim to harness collective phenomena like superradiance for fast and efficient energy storage and delivery [8,9]. Substantial progress has been made in this direction, both experimentally [10–13] and theoretically [14,15]. However, capturing the many-body physics of these complex systems remains challenging.

Existing theoretical studies of light-matter hybrid systems commonly rely on two classes of approximations, leading to simplified models such as the Dicke and extended Bose-Hubbard models. The Dicke model retains the photonic degree of freedom but neglects interactions inside the matter system, simplifying it into a collection of noninteracting two-level qubits coupled to a shared photon mode [10,14,16–19]. Although widely adopted in quantum battery and circuit QED studies, the neglected interactions are intrinsic and usually unavoidable in real systems. These interactions originate from multiple mechanisms: in circuit QED, capacitive couplings among qubits give rise to tunable ferromagnetic or antiferromagnetic interactions [20–24]; in optical cavity QED, dipole-dipole interactions among atoms or molecules lead to short-range spin-exchange terms across optical lattices or tweezer arrays [25,26]; and in quantum batteries, electronic tunneling and molecular interactions generate similar short-range couplings [27–30]. These interactions can substantially reshape the emergent phases and alter the performance of quantum devices [31].

On the other hand, the extended Bose-Hubbard model treats matter degrees of freedom explicitly while integrating out the photonic field, thereby reducing the problem to a competition between short-range and photon-mediated long-range interactions [32–35]. However, this framework cannot capture superradiant effects, which requires retaining the polaritonic wave function [36–38].

To overcome the limitations of simplified models and explore the rich many-body physics arising from both light-matter and matter-matter interactions, it is thus needed to incorporate interactions among the matter degrees of freedom (see Fig. 1). In order to simulate the strong-coupling regime efficiently, in this Letter we develop a hybrid numerical approach that combines a variational polaritonic dressing with an exact many-body solver for the matter subsystem, thereby going beyond mean-field approximations. This framework allows us to treat both light-induced collective effects and interaction-driven correlations on equal footing. Thus, we identify the impact of different types of interactions on the ground-state phases: in the Dicke-Ising model, we observe both first- and second-order phase transitions into the superradiant phase, while in the Dicke-XXZ model, we reveal a coexistence phase featuring XY spin order and superradiance. In both cases, superradiant signatures are significantly enhanced relative to those in the standard Dicke model.

[*]Contact author: jpedromend@gmail.com
[†]Contact author: Krzysztof.Jachymski@fuw.edu.pl
[‡]Contact author: yao.wang@emory.edu

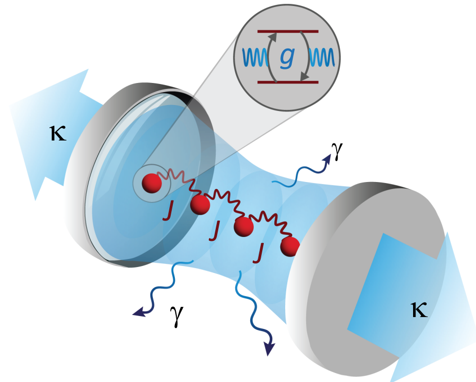

FIG. 1. Schematic of the Dicke-Heisenberg model. The system comprises an ensemble of two-level qubits, embedded in an optical cavity. They interact anisotropically with their nearest neighbors through an exchange interaction $\mathbf{J}$ and couple collectively to a single cavity mode with strength g. Dissipative effects include photon loss at rate κ and spontaneous emission at rate γ, both of which are assumed to be slow compared to the coherent coupling (i.e., $g^2 \gg 2\gamma\kappa$).

The extended model we consider, referred to as the Dicke-Heisenberg model, is described by the Hamiltonian

$$\mathcal{H} = \omega a^\dagger a + \varepsilon \sum_{i=1}^{N} s_i^z + \frac{2g}{\sqrt{N}} \sum_{i=1}^{N} s_i^x (a + a^\dagger) - \sum_{\langle i,j \rangle =1} \sum_{\alpha=x,y,z} J_\alpha s_i^{(\alpha)} s_j^{(\alpha)}, \quad (1)$$

where the first three terms correspond to the standard Dicke model [39–41] and the final term reflects interactions among the matter degrees of freedom [42]. Each two-level matter component, separated by energy ε, is encoded as a local spin-$1/2$ operator s_n^α. For clarity and generality, we refer to these two-level systems as "spins" throughout, although they may represent atomic orbitals, molecular states, or superconducting qubits in experimental implementations. The operators a and $a^\dagger$ denote photon annihilation and creation operators, respectively, with a fixed frequency ω. g is the light-matter interaction strength and N is the system size. We set $\omega = \varepsilon = 1$ throughout this Letter.

Numerical approach—The model in Eq. (1) that combines spins and photons poses considerable numerical challenges due to the distinct physical nature of their constituent subsystems. Interacting spins exhibit strong correlations that demand quantum many-body computational techniques [43–49]. In contrast, the photon subsystem inhabits an infinite-dimensional Hilbert space, with occupation numbers that can grow significantly in superradiant or polaronic regimes. Direct truncation of the bosonic space quickly becomes unreliable. However, the photonic field is typically highly coherent, with weak internal entanglement, suggesting that variational methods can effectively capture its wave function [50,51].

A practical strategy for addressing strong coupling in such composite systems involves a variational unitary transformation, i.e., the polaritonic dressing, which displaces the photon field in a way that depends on the many-body state of the spins [52–54]. This transformation rotates the system into a frame where spin and photon wave functions are approximately separable. Here, we apply this hybrid variational method to the models defined in Eq. (1). Specifically, the hybrid numerical approach adopted here leverages a non-Gaussian state (NGS) ansatz, $|\psi\rangle = U_\lambda(|\psi_{\mathrm{ph}}\rangle \otimes |\phi\rangle)$, where $|\psi_{\mathrm{ph}}\rangle$ describes the photonic degrees of freedom, $|\phi\rangle$ is a many-body spin wave function, and U_λ is a non-Gaussian unitary entangling transformation that encodes polaritonic correlations. The photon state $|\psi_{\mathrm{ph}}\rangle$ is approximated by a Gaussian state $|\psi_{\mathrm{ph}}\rangle = e^{i\boldsymbol{R}^T\sigma\boldsymbol{\Delta}_R} e^{-(i/2)\boldsymbol{R}^T\boldsymbol{\xi}\boldsymbol{R}}|0\rangle$, where $\mathbf{R} = (x, p)^T$ represents the bosonic quadrature vector. The photon displacement is generated by $\boldsymbol{\Delta}_R$ and squeezing is induced by $\boldsymbol{\xi}$ [55]. The NGS transformation U_λ introduces entanglement between photons and spins:

$$U_\lambda = \exp\left\{-\lambda \sum_i s_i^x (a^\dagger - a)\right\}. \quad (2)$$

The variational parameter λ controls the polaritonic dressing and is determined self-consistently along with the photon variational parameters described below.

The variational ground state of the Dicke-Heisenberg model is obtained by minimizing the total energy $\mathcal{E}(\boldsymbol{\Delta}_R, \boldsymbol{\xi}, \lambda, |\phi\rangle) = \langle\psi|\mathcal{H}|\psi\rangle$. This is accomplished using a self-consistent approach involving two coupled optimization procedures. The first step minimizes the energy with respect to the variational parameters $\boldsymbol{\Delta}_R, \boldsymbol{\xi}$, and λ, which determine the NGS transformation and the photon state. By fixing these variational parameters, the second step numerically calculates the ground state $|\phi\rangle$ of the effective spin Hamiltonian $H_{\mathrm{eff}}(\boldsymbol{\Delta}_R, \boldsymbol{\xi}, \lambda) = \langle\psi_{\mathrm{ph}}|U_\lambda^\dagger H U_\lambda|\psi_{\mathrm{ph}}\rangle$, which is renormalized by the above transformations [56–62], via density matrix renormalization group (DMRG). This numerical simulation is conducted only for the spin subsystem without the necessity of truncating the photonic Hilbert space. Together, these two updates form a single self-consistent iteration, ensuring the energy decrease, which is repeated until convergence. This method ensures that even when the physical photon number becomes large—as is typical in superradiant regimes—the bosonic fluctuations in the transformed frame remain small and numerically tractable. Thus, it enables an accurate and efficient solution for strongly coupled systems with many-body effects (see further analysis in Supplemental Material [63]).

In this Letter, we restrict our analysis to a one-dimensional chain with nearest-neighbor spin interactions, a geometry naturally compatible with DMRG due to its low entanglement scaling and efficient tensor network representation [66]. While exact diagonalization has previously proven efficient for hybrid NGS approaches in electron-phonon systems [53,67], DMRG offers significant advantages for models such as the Dicke-XXZ model, particularly when extrapolating to the thermodynamic limit becomes essential.

We first benchmark the hybrid variational framework on the standard Dicke model by setting all spin-spin interactions to zero ($J_\alpha = 0$). This serves as a useful test case, allowing direct comparison with analytically known results. We monitor key physical quantities, including the ground-state energy, average photon number, and magnetization. Our simulations capture the well-established superradiant phase transition at $g_c = \sqrt{\omega\epsilon}/2$ in the large-N limit, as shown in Figs. 2(a) and 2(b). The magnetization, $M_z = \sum_i \langle s_i^z \rangle / N$, and per-site photon occupation $\langle n \rangle / N$ transition sharply across the critical point [68]: from a finite M_z and vanishing $\langle n \rangle / N$ in the normal phase to a vanishing M_z and sizable $\langle n \rangle / N$ in the superradiant phase. As expected, the total photon number is size independent (equivalently, $\langle n \rangle / N \approx 0$) in the normal phase, while scaling linearly with N in the superradiant regime, consistent with $\langle n \rangle \propto N$. In addition, because the Dicke model without spin-spin interactions possesses permutation symmetry, its ground state can be solved analytically in the thermodynamic limit via Holstein-Primakoff transformation [41,63]. Our numerical simulations converge toward the analytic coherent-state solution as N increases, validating the accuracy of the hybrid method across both finite-size and thermodynamic regimes.

Dicke–Ising model—Building on the benchmark analysis of the standard Dicke model, we now incorporate spin-spin interactions and investigate the resulting phase diagram of the Dicke-Ising model. These nonperturbative interactions explicitly break permutation symmetry and further reduce residual spin symmetries, which directly affects the superradiant properties and places the model beyond the reach of perturbative or mean-field approximations. To isolate the impact of Ising-like couplings, we set $J_x = J_y = 0$ and $J_z = 4J$. As illustrated in Fig. 3(a), the inclusion of spin-spin interactions leads to significant restructuring of the phase diagram, giving rise to three distinct phases described below.

Starting from the standard Dicke limit ($J = 0$), marked by the vertical arrow in Fig. 3(c), the critical coupling g_c acquires a J dependence described by $g_c(J) = \sqrt{\omega\epsilon/4 + \omega J}$ [63]. Notably, g_c decreases as J

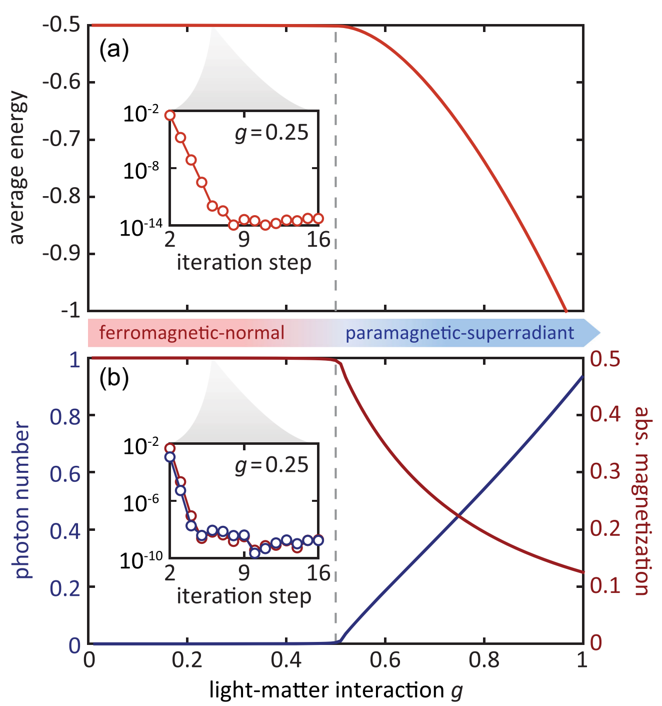

FIG. 2. Ground-state properties of the Dicke model obtained via the hybrid variational method. (a) Average energy and (b) average photon occupation and absolute magnetization. Simulations are performed for $N = 200$. The insets show the iteration errors at each step of the self-consistent iterations for the representative case $g = 0.25$ system. The energy is converged to a threshold of 10^{-12}, while photon number and magnetization are converged to 10^{-8}.

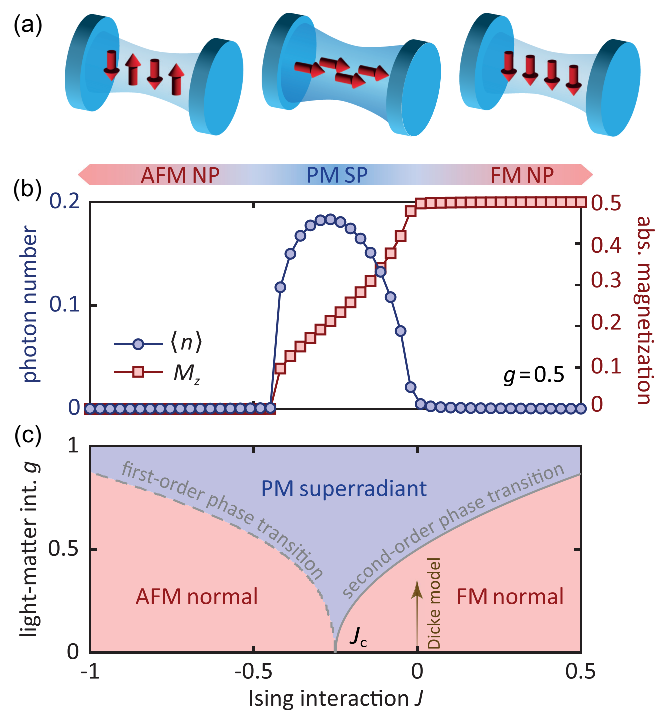

FIG. 3. (a) Representative spin configurations in phases of the Dicke-Ising model. (b) Magnetization and average photon number calculated for $g = 0.5$ and $N = 100$. (c) Phase diagram of the Dicke-Ising model, where the solid (dashed) lines denote second-order (first-order) transitions between the normal and superradiant phases. The normal phase is further divided by a critical coupling J_c into regions with distinct spin configurations. The vertical arrow marks the Dicke model.

becomes negative and vanishes at $J = -\varepsilon/4$, which defines a critical coupling J_c. This separates the normal phase into a ferromagnetic-normal (FM NP) phase for $J > J_c$ and an antiferromagnetic-normal (AFM NP) phase for $J < J_c$.

On the FM NP side ($J > J_c$), the transition into the superradiant phase resembles that of the standard Dicke model. As the light-matter coupling g exceeds the renormalized threshold $g_c(J)$, the system undergoes a continuous phase transition from the normal phase to the superradiant phase, now termed the paramagnetic-superradiant (PM SP) phase to include the spin configuration. The latter is characterized by a vanishing spin order and finite photon occupation. Alternatively, for a fixed g within the normal phase, decreasing J across the phase boundary leads to a continuous decline in magnetization [see Fig. 3(b)], confirming the FM PM second-order transition and reflecting the underlying symmetry-breaking mechanism. This finding contrasts with a recent conclusion obtained by small-size exact diagonalization with Hilbert space truncation [69], which interpreted the transition as first order. Our simulations extrapolate to the thermodynamic limit and resolve this discrepancy, showing that the FM NP to PM SP transition remains second order, consistent with the standard Dicke model. This conclusion is corroborated by a mean-field analysis in the thermodynamic limit, where the impact of the Ising interaction can be effectively absorbed by renormalizing the level splitting as $\varepsilon_{\mathrm{eff}} = \varepsilon + 4J$, consistent with the observed $g_c(J)$ [63].

An important consequence of introducing spin-spin interactions is the substantial enhancement of photon number in the superradiant phase. As demonstrated in Fig. 3(b), for $g = 0.5$, which coincides with the critical coupling $g_c(J = 0)$ of the standard Dicke model marking the onset of superradiance, the per-site averaged photon number increases markedly with moderate negative values of J, reaching nearly 0.2. This enhancement can be understood as a consequence of the renormalized critical threshold: negative J lowers the effective g_c, shifting the system deeper into the superradiant regime at fixed g. This mechanism provides a practical route for engineering enhanced superradiant states through moderate spin-spin interactions. However, the effect is not unbounded. As illustrated in Fig. 3(b), further decreasing J beyond -0.27 causes the photon number to decrease. Thus, an optimal interaction strength exists that maximizes superradiance at a given light-matter coupling. Beyond this point, stronger interactions destabilize the superradiant state due to the onset of a competing phase.

On the AFM NP side ($J < J_c$), the system exhibits qualitatively different behavior from that of the standard Dicke model. As shown in Fig. 3(b), reducing J beyond a secondary threshold (~ -0.43 for $g = 0.5$) results in a sharp, discontinuous jump in key observables, indicating a first-order phase transition. Although this phase lacks superradiance, with vanishing photon occupation, it is distinct from both the Dicke normal phase and the FM NP regime due to its internal spin structure. Specifically, the spin subsystem exhibits long-range antiferromagnetic order, as confirmed by staggered spin correlations $\langle (-1)^r s_i^z s_{i+r}^z \rangle = 1/4$. Because the AFM and superradiant phases break fundamentally different symmetries (translational and parity, respectively), they cannot be adiabatically connected by a continuous phase transition. Therefore, unlike the FM NP, where the interaction simply renormalizes the level splitting, the AFM NP to PM SP reflects a discontinuous change in symmetry of the ground state. This behavior contrasts with a recent variational mean-field study that reported a phase with coexisting AFM order and superradiance [21]. With careful tuning of parameters and extrapolation to the thermodynamic limit, our simulations do not observe such a coexistence phase. This discrepancy highlights the importance of treating the spin sector exactly: while the photonic sector is often well approximated by a coherent state, strongly correlated spin states may introduce significant effects [63].

Dicke-XXZ model—Beyond isotropic spin-spin couplings, many experimental systems naturally host anisotropic matter-matter interactions, arising from directional dipolar forces and anisotropic tunneling processes [26,70–72]. Motivated by these physical realizations, we further consider the Dicke-XXZ model, where $J_x = J_y = 1$ and J_z is a tunable anisotropy parameter. The distinction between the Dicke-Ising and Dicke-XXZ models primarily inherits from their different ground-state phase diagrams at zero light-matter coupling ($g = 0$). Whereas the Dicke-Ising model exhibits a single critical coupling J_c in Fig. 3, the XXZ model splits it into two critical couplings $J_c^{\mathrm{FM}} = 0$ and $J_c^{\mathrm{AFM}} \approx -2.8$ [73–76]. The intermediate phase is usually referred to as the gapless XY phase. The introduction of light-matter interaction further broadens up the intermediate phase: a finite photon occupation $\langle n \rangle / N$ emerges beyond these two critical couplings by destabilizing the FM and AFM orders, as shown in Fig. 4(a).

Within this intermediate region, where in-plane XY correlations dominate and the spin sector is paramagnetic, an infinitesimal light-matter interaction g is sufficient to induce divergence in the total photon number $\langle n \rangle$. While such divergence is a signature of superradiance, its manifestation here differs markedly from the standard Dicke or Dicke-Ising models, where the photon number per site saturates in the superradiant phase (see Figs. 2 and 3). Instead, due to persistent in-plane XY fluctuations, it displays sublinear scaling with system size: $\langle n \rangle / N \propto N^{-\alpha}$ with $0 \leq \alpha < 1$ [see Fig. 4(b)]. As the light-matter interaction g increases for a fixed J_z, the exponent α decreases continuously toward zero, suggesting a smooth evolution toward the conventional superradiant regime. For comparison, in the normal FM NP and AFM NP phases, we observe $\langle n \rangle / N \propto 1/N$, which implies a constant total

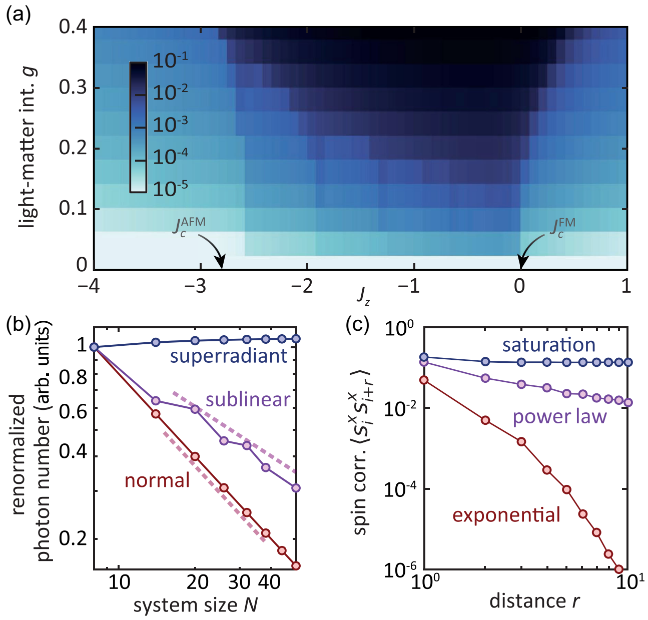

FIG. 4. Phases of the Dicke-XXZ model. (a) Photon number per site $\langle n\rangle/N$ for various J_z and g, obtained using $N=24$. The two arrows indicate the critical couplings at zero light-matter coupling ($g=0$). (b) Scaling laws of $\langle n\rangle/N$ in different phases: the normal phase (red, $J_z=1$, $g=0.01$) exhibits a $\langle n\rangle/N\propto 1/N$ decay; the superradiant phase (blue, $J_z=-1.6$, $g=0.4$) shows $\langle n\rangle\propto N$; a sublinear scaling arises in the intermediate regime (purple, $J_z=-1.6$, $g=0.01$). (c) Spatial profile of the spin-spin correlation $\langle s_i^x s_{i+r}^x\rangle$ for $N=32$. Deep in the normal phase (red, $J_z=-5$, $g=0.01$) it decays exponentially, while the superradiant phase supports long-range order. The intermediate regime displays power-law decay, consistent with quasi-long-range XY-type order [blue and purple the same as in (b)].

photon number but vanishing per-site occupation in the thermodynamic limit.

The coexistence of spin correlations and photon superradiance is another distinctive feature of this intermediate phase. In Fig. 4(c), the in-plane spin correlations $\langle s_i^x s_{i+r}^x\rangle$ decay exponentially in the normal phases, where z-axis FM or AFM order dominates. In contrast, within the XY phase, the correlations follow a power-law decay, indicating quasi-long-range order. Although the photon field breaks rotational symmetry in the xy plane by favoring s^x polarization, it does not destroy the XY correlations. Instead, the power-law character persists across the superradiant regime and smoothly evolves into long-range order as g increases, consistent with the Dicke-Ising-like superradiant phase [see Fig. 4(c)].

In conclusion, we have explored how matter-matter interactions shape the phases of strongly coupled light-matter systems described by Dicke-like models, employing a hybrid method that combines variational non-Gaussian states with DMRG. This framework captures both strong light-matter coupling and strong correlations on equal footing, extending the understanding of such systems well beyond mean-field or perturbative treatments (see demonstrations in SM [63]). Our simulations reveal two distinct types of phase boundaries induced by Ising-type interactions: one that adiabatically shifts the conventional superradiant boundary, and another that produces a qualitatively different normal phase characterized by antiferromagnetic order and first-order transition to superradiance. Introducing anisotropic interactions further enriches the phase diagram, leading to a strongly correlated intermediate regime where in-plane spin order coexists with superradiance. These results highlight the intricate effects of matter interactions and the necessity of many-body approaches.

Acknowledgments—J. P. M. and K. J. were supported by the Polish National Agency for Academic Exchange (NAWA) via the Polish Returns 2019 program and acknowledge Polish high-performance computing infrastructure PLGrid (HPC Center: ACK Cyfronet AGH) for providing computer facilities and support within computational Grant No. PLG/2024/017478. Y. W. acknowledges the support by the U.S. Department of Energy, Office of Science, Basic Energy Sciences, under Early Career Award No. DE-SC0024524.

Data availability—The data that support the findings of this article are not publicly available. The data are available from the authors upon reasonable request.

[1] A. G. J. MacFarlane, J. P. Dowling, and G. J. Milburn, Quantum technology: The second quantum revolution, Phil. Trans. R. Soc. A **361**, 1655 (2003).
[2] B. Julsgaard, J. Sherson, J. I. Cirac, J. Fiurášek, and E. S. Polzik, Experimental demonstration of quantum memory for light, Nature (London) **432**, 482 (2004).
[3] H. J. Kimble, The quantum internet, Nature (London) **453**, 1023 (2008).
[4] H. Ritsch, P. Domokos, F. Brennecke, and T. Esslinger, Cold atoms in cavity-generated dynamical optical potentials, Rev. Mod. Phys. **85**, 553 (2013).
[5] A. Reiserer and G. Rempe, Cavity-based quantum networks with single atoms and optical photons, Rev. Mod. Phys. **87**, 1379 (2015).
[6] G. Findik, M. Biliroglu, D. Seyitliyev, J. Mendes, A. Barrette, H. Ardekani, L. Lei, Q. Dong, F. So, and K. Gundogdu, High-temperature superfluorescence in methyl ammonium lead iodide, Nat. Photonics **15**, 676 (2021).
[7] P. Forn-Díaz, L. Lamata, E. Rico, J. Kono, and E. Solano, Ultrastrong coupling regimes of light-matter interaction, Rev. Mod. Phys. **91**, 025005 (2019).
[8] F. Campaioli, S. Gherardini, J. Q. Quach, M. Polini, and G. M. Andolina, Colloquium: Quantum batteries, Rev. Mod. Phys. **96**, 031001 (2024).
[9] S. Julià-Farré, T. Salamon, A. Riera, M. N. Bera, and M. Lewenstein, Bounds on the capacity and power of quantum batteries, Phys. Rev. Res. **2**, 023113 (2020).

[10] J. Q. Quach, K. E. McGhee, L. Ganzer, D. M. Rouse, B. W. Lovett, E. M. Gauger, J. Keeling, G. Cerullo, D. G. Lidzey, and T. Virgili, Superabsorption in an organic microcavity: Toward a quantum battery, Sci. Adv. **8**, eabk3160 (2022).

[11] J. Joshi and T. S. Mahesh, Experimental investigation of a quantum battery using star-topology NMR spin systems, Phys. Rev. A **106**, 042601 (2022).

[12] C.-K. Hu, J. Qiu, P. J. P. Souza, J. Yuan, Y. Zhou, L. Zhang, J. Chu, X. Pan, L. Hu, J. Li, Y. Xu, Y. Zhong, S. Liu, F. Yan, D. Tan, R. Bachelard, C. J. Villas-Boas, A. C. Santos, and D. Yu, Optimal charging of a superconducting quantum battery, Quantum Sci. Technol. **7**, 045018 (2022).

[13] K. Baumann, C. Guerlin, F. Brennecke, and T. Esslinger, Dicke quantum phase transition with a superfluid gas in an optical cavity, Nature (London) **464**, 1301 (2010).

[14] D. Ferraro, M. Campisi, G. M. Andolina, V. Pellegrini, and M. Polini, High-power collective charging of a solid-state quantum battery, Phys. Rev. Lett. **120**, 117702 (2018).

[15] H.-L. Shi, S. Ding, Q.-K. Wan, X.-H. Wang, and W.-L. Yang, Entanglement, coherence, and extractable work in quantum batteries, Phys. Rev. Lett. **129**, 130602 (2022).

[16] F. Dimer, B. Estienne, A. S. Parkins, and H. J. Carmichael, Proposed realization of the Dicke-model quantum phase transition in an optical cavity QED system, Phys. Rev. A **75**, 013804 (2007).

[17] M. P. Baden, K. J. Arnold, A. L. Grimsmo, S. Parkins, and M. D. Barrett, Realization of the Dicke model using cavity-assisted raman transitions, Phys. Rev. Lett. **113**, 020408 (2014).

[18] Z. Zhang, C. H. Lee, R. Kumar, K. J. Arnold, S. J. Masson, A. L. Grimsmo, A. S. Parkins, and M. D. Barrett, Dicke-model simulation via cavity-assisted raman transitions, Phys. Rev. A **97**, 043858 (2018).

[19] A. Crescente, M. Carrega, M. Sassetti, and D. Ferraro, Ultrafast charging in a two-photon Dicke quantum battery, Phys. Rev. B **102**, 245407 (2020).

[20] Y. A. Pashkin, T. Yamamoto, O. Astafiev, Y. Nakamura, D. V. Averin, and J. S. Tsai, Quantum oscillations in two coupled charge qubits, Nature (London) **421**, 823 (2003).

[21] Y. Zhang, L. Yu, J.-Q. Liang, G. Chen, S. Jia, and F. Nori, Quantum phases in circuit QED with a superconducting qubit array, Sci. Rep. **4**, 4083 (2014).

[22] T. Jaako, Z.-L. Xiang, J. J. Garcia-Ripoll, and P. Rabl, Ultrastrong-coupling phenomena beyond the Dicke model, Phys. Rev. A **94**, 033850 (2016).

[23] D. De Bernardis, T. Jaako, and P. Rabl, Cavity quantum electrodynamics in the nonperturbative regime, Phys. Rev. A **97**, 043820 (2018).

[24] O. Viehmann, J. von Delft, and F. Marquardt, Superradiant phase transitions and the standard description of circuit QED, Phys. Rev. Lett. **107**, 113602 (2011).

[25] M. T. Manzoni, L. Mathey, and D. E. Chang, Designing exotic many-body states of atomic spin and motion in photonic crystals, Nat. Commun. **8**, 14696 (2017).

[26] S. Whitlock, A. W. Glaetzle, and P. Hannaford, Simulating quantum spin models using Rydberg-excited atomic ensembles in magnetic microtrap arrays, J. Phys. B **50**, 074001 (2017).

[27] F.-Q. Dou, Y.-Q. Lu, Y.-J. Wang, and J.-A. Sun, Extended Dicke quantum battery with interatomic interactions and driving field, Phys. Rev. B **105**, 115405 (2022).

[28] F.-Q. Dou, H. Zhou, and J.-A. Sun, Cavity Heisenberg-spin-chain quantum battery, Phys. Rev. A **106**, 032212 (2022).

[29] W. Zhang, S. Wang, C. Wu, and G. Wang, Quantum battery based on dipole-dipole interaction and external driving field, Phys. Rev. E **107**, 054125 (2023).

[30] J. Wen, Z. Wen, P. Peng, and G.-Q. Li, Dicke-ising quantum battery of an ion chain driven by a mechanical oscillator, arXiv:2502.08065.

[31] F. Mivehvar, F. Piazza, T. Donner, and H. Ritsch, Cavity QED with quantum gases: New paradigms in many-body physics, Adv. Phys. **70**, 1 (2021).

[32] D. Nagy, G. Szirmai, and P. Domokos, Self-organization of a Bose-Einstein condensate in an optical cavity, Eur. Phys. J. D **48**, 127 (2008).

[33] N. Dogra, F. Brennecke, S. D. Huber, and T. Donner, Phase transitions in a Bose-Hubbard model with cavity-mediated global-range interactions, Phys. Rev. A **94**, 023632 (2016).

[34] S. Sharma, S. B. Jäger, R. Kraus, T. Roscilde, and G. Morigi, Quantum critical behavior of entanglement in lattice bosons with cavity-mediated long-range interactions, Phys. Rev. Lett. **129**, 143001 (2022).

[35] R. Landig, L. Hruby, N. Dogra, M. Landini, R. Mottl, T. Donner, and T. Esslinger, Quantum phases from competing short- and long-range interactions in an optical lattice, Nature (London) **532**, 476 (2016).

[36] A. V. Bezvershenko, C.-M. Halati, A. Sheikhan, C. Kollath, and A. Rosch, Dicke transition in open many-body systems determined by fluctuation effects, Phys. Rev. Lett. **127**, 173606 (2021).

[37] G. Orso, J. Zakrzewski, and P. Deuar, Self-organized cavity bosons beyond the adiabatic elimination approximation, Phys. Rev. Lett. **134**, 183405 (2025).

[38] L. Tolle, A. Sheikhan, T. Giamarchi, C. Kollath, and C.-M. Halati, Fluctuation-induced bistability of fermionic atoms coupled to a dissipative cavity, Phys. Rev. Lett. **134**, 133602 (2025).

[39] R. H. Dicke, Coherence in spontaneous radiation processes, Phys. Rev. **93**, 99 (1954).

[40] A. Safavi-Naini, R. J. Lewis-Swan, J. G. Bohnet, M. Gärttner, K. A. Gilmore, J. E. Jordan, J. Cohn, J. K. Freericks, A. M. Rey, and J. J. Bollinger, Verification of a many-ion simulator of the Dicke model through slow quenches across a phase transition, Phys. Rev. Lett. **121**, 040503 (2018).

[41] P. Kirton, M. M. Roses, J. Keeling, and E. G. Dalla Torre, Introduction to the Dicke model: From equilibrium to nonequilibrium, and vice versa, Adv. Quantum Technol. **2**, 1800043 (2019).

[42] D. C. Mattis, Ferromagnetism and spin waves in the band theory, Phys. Rev. **132**, 2521 (1963).

[43] S. R. White, Density matrix formulation for quantum renormalization groups, Phys. Rev. Lett. **69**, 2863 (1992).

[44] S. R. White, Density-matrix algorithms for quantum renormalization groups, Phys. Rev. B **48**, 10345 (1993).

[45] A. Wietek and A. M. Läuchli, Sublattice coding algorithm and distributed memory parallelization for large-scale exact

diagonalizations of quantum many-body systems, Phys. Rev. E **98**, 033309 (2018).
[46] A. M. Läuchli, J. Sudan, and R. Moessner, $s = \frac{1}{2}$ kagome Heisenberg antiferromagnet revisited, Phys. Rev. B **100**, 155142 (2019).
[47] S. J. Evered, D. Bluvstein, M. Kalinowski, S. Ebadi, T. Manovitz, H. Zhou, S. H. Li, A. A. Geim, T. T. Wang, N. Maskara, H. Levine, G. Semeghini, M. Greiner, V. Vuletić, and M. D. Lukin, High-fidelity parallel entangling gates on a neutral-atom quantum computer, Nature (London) **622**, 268 (2023).
[48] I. Cong, H. Levine, A. Keesling, D. Bluvstein, S.-T. Wang, and M. D. Lukin, Hardware-efficient, fault-tolerant quantum computation with Rydberg atoms, Phys. Rev. X **12**, 021049 (2022).
[49] A. Browaeys and T. Lahaye, Many-body physics with individually controlled Rydberg atoms, Nat. Phys. **16**, 132 (2020).
[50] T. Guaita, L. Hackl, T. Shi, C. Hubig, E. Demler, and J. I. Cirac, Gaussian time-dependent variational principle for the Bose-Hubbard model, Phys. Rev. B **100**, 094529 (2019).
[51] A. Christianen, J. I. Cirac, and R. Schmidt, Bose polaron and the Efimov effect: A gaussian-state approach, Phys. Rev. A **105**, 053302 (2022).
[52] H. Fehske, H. Röder, G. Wellein, and A. Mistriotis, Hole-polaron formation in the two-dimensional Holstein *t-J* model: A variational Lanczos study, Phys. Rev. B **51**, 16582 (1995).
[53] Y. Wang, I. Esterlis, T. Shi, J. I. Cirac, and E. Demler, Zero-temperature phases of the two-dimensional Hubbard-Holstein model: A non-Gaussian exact diagonalization study, Phys. Rev. Res. **2**, 043258 (2020).
[54] Y. Wang, T. Shi, and C.-C. Chen, Fluctuating nature of light-enhanced *d*-wave superconductivity: A time-dependent variational non-Gaussian exact diagonalization study, Phys. Rev. X **11**, 041028 (2021).
[55] T. Shi, E. Demler, and J. Ignacio Cirac, Variational study of fermionic and bosonic systems with non-gaussian states: Theory and applications, Ann. Phys. (Amsterdam) **390**, 245 (2018).
[56] Y. Takada and A. Chatterjee, Possibility of a metallic phase in the charge-density-wave–spin-density-wave crossover region in the one-dimensional Hubbard-Holstein model at half filling, Phys. Rev. B **67**, 081102(R) (2003).
[57] S. Reja, S. Yarlagadda, and P. B. Littlewood, Phase diagram of the one-dimensional Hubbard-Holstein model at quarter filling, Phys. Rev. B **84**, 085127 (2011).
[58] S. Karakuzu, L. F. Tocchio, S. Sorella, and F. Becca, Superconductivity, charge-density waves, antiferromagnetism, and phase separation in the Hubbard-Holstein model, Phys. Rev. B **96**, 205145 (2017).
[59] T. Ohgoe and M. Imada, Competition among superconducting, antiferromagnetic, and charge orders with intervention by phase separation in the 2d Holstein-Hubbard model, Phys. Rev. Lett. **119**, 197001 (2017).
[60] S. Reja and S. Nishimoto, Phase diagram of the Hubbard-Holstein model on a four-leg tube system at quarter filling, Phys. Rev. B **97**, 245108 (2018).
[61] Z. Han, S. A. Kivelson, and P. A. Volkov, Quantum bipolaron superconductivity from quadratic electron-phonon coupling, Phys. Rev. Lett. **132**, 226001 (2024).
[62] B. Min, Y. Zhang, Y. Guo, D. Segal, and Y. Ashida, Mixed-state phase transitions in spin-holstein models, Phys. Rev. B **111**, 115123 (2025).
[63] See Supplemental Material at http://link.aps.org/supplemental/10.1103/z8gv-7yyk for discussion of the mean-field approach to the Dicke-Ising model, analysis of beyond-mean-field effects, and benchmarks of the numerical methods, which includes Refs. [64,65]
[64] T. Holstein and H. Primakoff, Field dependence of the intrinsic domain magnetization of a ferromagnet, Phys. Rev. **58**, 1098 (1940).
[65] D. A. R. Sakthivadivel, Magnetisation and mean field theory in the Ising model, SciPost Phys. Lect. Notes 35 (2022).
[66] M. Fishman, S. R. White, and E. M. Stoudenmire, The ITensor Software Library for tensor network calculations, SciPost Phys. Codebases **2022**, 4 (2022).
[67] Y. Wang, Z. Chen, T. Shi, B. Moritz, Z.-X. Shen, and T. P. Devereaux, Phonon-mediated long-range attractive interaction in one-dimensional cuprates, Phys. Rev. Lett. **127**, 197003 (2021).
[68] As the system maps onto a spin chain, we adopt magnetic terminology to describe observables without loss of generality, although the matter degrees of freedom can be nonmagnetic in specific systems.
[69] J. Rohn, M. Hörmann, C. Genes, and K. P. Schmidt, Ising model in a light-induced quantized transverse field, Phys. Rev. Res. **2**, 023131 (2020).
[70] A. Micheli, G. K. Brennen, and P. Zoller, A toolbox for lattice-spin models with polar molecules, Nat. Phys. **2**, 341 (2006).
[71] A. de Paz, A. Sharma, A. Chotia, E. Maréchal, J. H. Huckans, P. Pedri, L. Santos, O. Gorceix, L. Vernac, and B. Laburthe-Tolra, Nonequilibrium quantum magnetism in a dipolar lattice gas, Phys. Rev. Lett. **111**, 185305 (2013).
[72] A. Browaeys, D. Barredo, and T. Lahaye, Experimental investigations of dipole-dipole interactions between a few Rydberg atoms, J. Phys. B **49**, 152001 (2016).
[73] L. Justino and T. R. de Oliveira, Bell inequalities and entanglement at quantum phase transitions in the *XXZ* model, Phys. Rev. A **85**, 052128 (2012).
[74] A. Niezgoda, M. Panfil, and J. Chwedeńczuk, Quantum correlations in spin chains, Phys. Rev. A **102**, 042206 (2020).
[75] C. N. Yang and C. P. Yang, One-dimensional chain of anisotropic spin-spin interactions. I. Proof of Bethe's hypothesis for ground state in a finite system, Phys. Rev. **150**, 321 (1966).
[76] C. N. Yang and C. P. Yang, One-dimensional chain of anisotropic spin-spin interactions. II. Properties of the ground-state energy per lattice site for an infinite system, Phys. Rev. **150**, 327 (1966).